Available online at www.sciencedirect.com
SCIENCE DIRECT®
International Journal of Heat and Fluid Flow 24 (2003) 1–13
International Journal of HEAT AND FLUID FLOW
www.elsevier.com/locate/ijhff

The development of a pulsed-wire probe for measuring flow velocity with a wide bandwidth

F. Durst [a], A. Al-Salaymeh [a,b,*], P. Bradshaw [a,1], J. Jovanović [a]

[a] Lehrstuhl für Strömungsmechanik, Universität Erlangen-Nürnberg, Cauerstraße 4, D-91058 Erlangen, Germany
[b] Mechanical Engineering Department, Faculty of Engineering and Technology, University of Jordan, Amman 11942, Jordan

Received 12 January 2002; accepted 4 August 2002

Abstract

The velocity range of a "time-of-flight" thermal flowmeter for slowly time varying flows can be increased by using wires (or other heating/sensing elements) with large thermal inertia (time constant) and heating the sending wire with a continuous periodic current, instead of discrete square-wave pulses as in the usual pulsed-wire anemometer. Because the time constants increase as the flow speed decreases, the time lag due to thermal inertia supplements the time lag due to the true time of flight, thus increasing the speed range/sensitivity of the device, especially at the low-speed end. The "output" is the phase shift between the current to the sending wire and the temperature of the receiving wire. The latter basically acts as a resistance thermometer. The device described here is for mainly unidirectional internal flows, and uses two parallel wires of 12.5 μm diameter. The usable speed range is 0.05–25 $m\,s^{-1}$ and the frequency response with 30 Hz excitation current is nominally 15 Hz.

Keywords: Flowmeter; Thermal flowmeter; Hot-wire anemometer

1. Introduction

This paper presents computations and experimental data to demonstrate increases in the useful speed range of "time-of-flight" heated-element flowmeters, of which the well-known pulsed-wire anemometer is a special case. In these devices the fluid flow speed, referred to as U in this paper, is inferred from the time difference Δt between the transient or periodic electrical heating of the upstream "sending" wire and the corresponding change in temperature of the "receiving" wire, located a distance Δx downstream of the sending wire. The traditional view of these devices is that the wires should be as thin as possible, so that thermal lag in the wires does not greatly influence the response. In this case it is expected that the time difference will be close to $\Delta t = \Delta x/U$. The main point of the present paper is that, for constant or slowly varying flow speed, the thermal lag of larger diameter wires can be beneficial and increases the range of flow speed over which a measurable response to flow can be obtained.

There are two main choices for the variation of heating current:

- By definition, the pulsed-wire anemometer (e.g. Handford and Bradshaw, 1989) uses square-wave pulses separated in time (by an amount at least as large as the wire time constant, so that the wire has time to cool between pulses). The time difference Δt is measured between the leading edge of the current pulse and the rise of the receiving wire temperature (resistance) through a threshold set slightly above ambient temperature. The finite threshold is needed so that natural air temperature fluctuations are not mistaken for the response to the sending wire, and the calibration depends significantly on the threshold. The pulse repetition rate is usually too slow to resolve the higher-frequency (shorter wavelength) fluctuations in a turbulent flow. However a pulse starting at time t gives a good approximation to the velocity time-averaged between t and $t + \Delta t$, which will in turn

* Corresponding author. Tel.: +49-91318529501; fax: +49-91318529503.
E-mail addresses: durst@lstm.uni-erlangen.de (F. Durst), salaymeh@ju.edu.jo (A. Al-Salaymeh), bradshaw@vonkarman.standford.edu (P. Bradshaw), jovan@lstm.uni-erlangen.de (J. Jovanović).
[1] Permanent address: Department of Mechanical Engineering, Stanford University, Stanford, CA 94305, USA.

0142-727X/02/$ - see front matter © 2002 Elsevier Science Inc. All rights reserved.
PII: S0142-727X(02)00203-5

Nomenclature

A_w	cross-sectional area of the wire (m^2)
c_w	specific heat of the wire material (J/(kg °C))
d_w	wire diameter (m)
f	frequency (Hz)
h	coefficient of convective heat transfer ($W/(m^2\,°C)$)
I	electrical current (A)
k_w	thermal conductivity of the wire (W/(m °C))
k_f	thermal conductivity of the fluid (W/(m °C))
M	time constant of the wire (s)
Nu	Nusselt number
Pe	Peclet number
Pr	Prandtl number
Re	Reynolds number
t	time (s)
Δt	time shift between the sending and the receiving signals (s)
Δt_f	time of flight (s)
T	temperature (°C)
T_a	ambient temperature (°C)
T_f	mean film temperature (°C)
T_w	wire temperature (°C)
ΔT_a	fluctuation of the ambient temperature (°C)
U	flow velocity (m/s)
U_∞	free stream velocity (m/s)
Δx	distance between the hot wires (m)
z	distance measured along the heated wire (m)
Greeks	
α_∞	wire temperature coefficient at fluid temperature ($°C^{-1}$)
Δ	difference operator
ε	emmisivity of the sensor wire
$\Delta\phi$	phase difference between the heated and the detected signal (rad)
ρ_w	density of the wire material (kg/m^3)
σ	Stefan–Boltzmann constant ($W/(m^2\,K^4)$)
ν	kinematic viscosity (m^2/s)
χ_w	resistivity of the wire material at the local wire temperature (Ω m)
ω	angular velocity (rad/s)

be a good approximation to the velocity at $t + \Delta t/2$ if typical frequencies are of smaller order than $1/\Delta t$. It can be seen that this is equivalent to a spatial resolution roughly equal to Δx. In its usual form, the pulsed-wire probe has three wires, with upstream and downstream receiving wires mounted with their axes normal to the axis of the sending wire. To a good approximation, the probe responds to the velocity component normal to both axes, and this is its main advantage over the hot-wire anemometer, whose directional sensitivity is more complicated.

- The alternative to using pulse heating and measuring directly is to use sinusoidal heating, at frequency f, say, and measure the phase difference between the heating current and the receiving wire temperature, nominally equal to $2\pi f\,\Delta x/U$ radians. This avoids the need for an arbitrary temperature threshold. Since the heat input varies as the square of the current it is simplest to add a dc component to the excitation current so that it never goes negative and frequency doubling is avoided. Again the heating-current period must not be too small compared to the sending-wire time constant, but this time the reason is to avoid severe attenuation of the temperature variation in the sending wire. Since the wire is not allowed to cool down completely between cycles its mean temperature is well above atmospheric. The first instrument of this kind was developed by Kovasznay (1949). Doubtless to avoid what would have been complicated electronics by the standards of 50 years ago, he did not measure the phase difference directly but measured the wavelength of the temperature variation in the wake of the sending wire by moving the receiving wire upstream and downstream.

The latter heating approach is chosen in this work.

2. The sinusoidally heated flowmeter

The present paper considers only the case of sinusoidal heating current (with a dc offset to avoid frequency doubling: for simplicity we will call this "sinusoidal" heating). Also, it discusses only two-wire probes, with the two wires parallel. Our immediate application is to measurements of volume flow rates in slowly changing unidirectional internal flows, which is why we call the device a "flowmeter" even though the primary response is to velocity. The extension to the three-wire case (for bidirectional flows) will be reported separately, but is trivial. The one-wire case, also to be reported separately, is discussed briefly at the end of this paper.

The main finding of the authors' is that the influence of the wire time constants on the measuring range of the flowsensor can be beneficial. Briefly, time constants of heated wires decrease as the flow speed increases, so the total phase shift decreases more rapidly than if the time constants were negligibly small. This means that the speed range over which useful signals are obtainable is increased. The acceptable range for the authors' probe is about 0.05–25 $m\,s^{-1}$, a ratio of 1:500. By contrast the speed range of Kovasznay (1949) device was from 0.3 to

Table 1
Sensor parameters

Sensor parameters	Values
Wire diameter, d_w	12.5 μm (platinum)
Wire length	5 mm
Wire spacing, Δx	1.5 mm
Excitation frequency	30 Hz
Peak excitation current	100 mA

3 m s^{-1} (only 1:10), and in a survey of patents for time-of-flight anemometers the greatest claim that was found corresponded to a speed range of less than 1:100. However, it should be mentioned that the definition of the usable speed range of a flowsensor is arbitrary: in this paper it is estimated as the range within which the resolution of the device is better than 3%. Collis and Williams (1959) empirical criterion for negligible buoyancy effects, where the Grashof number should be less than the cube root of the Reynolds number, suggests that buoyancy would become important only below 0.04 m s^{-1}, i.e. below the bottom of our usable range. For the present sensor developments the best conditions we found had an optimum wire diameter of about 12.5 μm (a standard size for commercially available platinum wire) with our chosen heating-current frequency of 30 Hz and a wire spacing of 1.5 mm. There seems to be no advantage in using different diameters for the sending and receiving wires. Clearly this is not a design for a fast-response device, but in principle similar probes with thinner wires, smaller spacing and higher excitation frequency could be made. For industrial or medical use, of course, thicker wires make a more rugged instrument. Unless otherwise stated, all results given below refer to the final "optimum" configuration given in Table 1. More details of our work are given in Durst et al. (2001) and in the Ph.D. thesis of Al-Salaymeh (2001).

Even in the case of a single wire, the decrease of wire time constant with increasing speed can be used to increase the speed range. Consider a single wire excited by discrete, widely separated, square waves of electrical current: then the maximum voltage attained by the wire depends both on its dynamic response ("time constant") and on the (mean) $\mathrm{d}Nu(Re)/\mathrm{d}Re$ relation. The time constant and the derivative both decrease with increasing flow speed so the two effects reinforce each other and lead to a usable speed range larger than that of a simple hot-wire flowmeter.

3. Theoretical investigations

3.1. Three contributions to time lag

The total time lag or phase shift is made up of (1) the thermal lag of the sending wire, (2) the true time of flight (convection by the fluid in the wake of the sending wire, with some effect of longitudinal heat diffusion at low speeds), and (3) the thermal lag of the receiving wire. The authors carried out numerical calculations of all three time lags over a range of parameters, taking account of variation of wire and fluid properties with temperature. As a result of these variations of influencing parameters, the system response to a sinusoidal heating current is not exactly sinusoidal especially at the high velocity range (Figs. 1 and 2): however, this does not affect the calibration procedure. The calculations to obtain the flow and heating response of the sensor are straightforward and we omit algebraic detail here. A fuller account is in Durst et al. (2001).

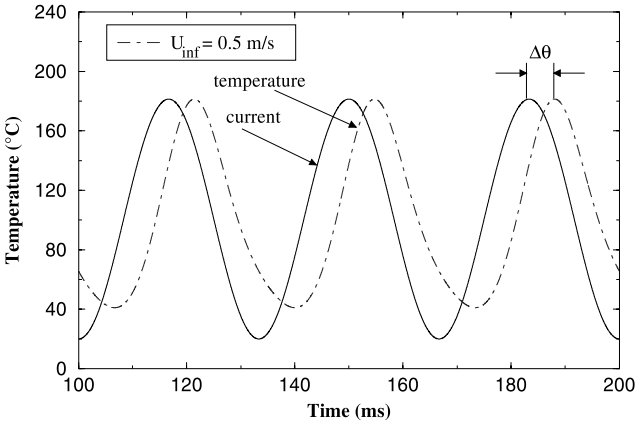

Fig. 1. The phase difference between the driving current signal and the output wire temperature at low flow velocity ($U_\infty = 0.5$ m s^{-1}).

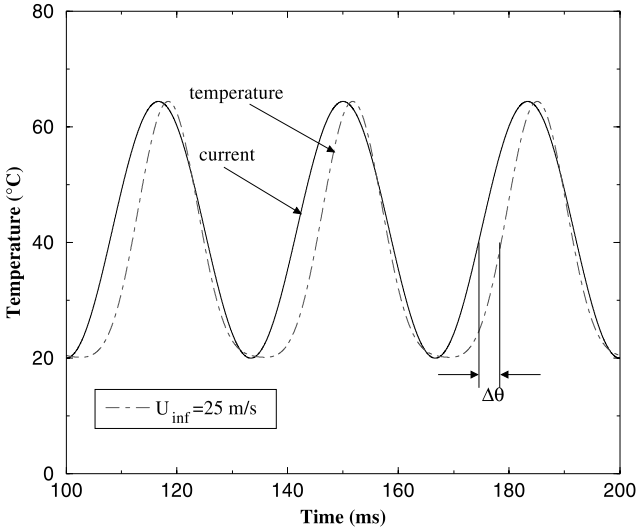

Fig. 2. The phase difference between the driving current signal and the output wire temperature at high flow velocity ($U_\infty = 25$ m s^{-1}).

3.2. Wire thermal response and forced convection

The rate of increase of wire temperature (thermal internal energy) with time depends on:

Ohmic heating by the excitation current, heat transfer to the fluid, radiation and heat conduction in the wire towards the end supports.

In the theoretical investigations, the sending wire was heated by a sinusoidally varying electrical current:

$$I(t) = I_0 + \Delta I \sin(2\pi f t) \tag{1}$$

The differential equation for the heat balance in the heated wire was derived to be:

$$\rho_w c_w A_w \frac{\partial T_w}{\partial t} = \frac{I^2 \chi_w}{A_w} - \pi d_w h (T_w - T_\infty) + k_w A_w \frac{\partial^2 T_w}{\partial z^2} - \pi d_w \sigma \varepsilon (T_w^4 - T_\infty^4) \tag{2}$$

Estimates of the magnitudes of the five terms show that the last two terms are negligible for the wire and flow conditions (wire length 5 mm, aspect ratio 400). Also, ohmic heating of the receiving wire by the current used to measure its resistance was small and in any case virtually independent of time. For convective heat transfer from or to the wire we have used the empirical formula of Collis and Williams (1959)

$$Nu = [0.24 + 0.56\,\mathrm{Re}^{0.45}] \left[\frac{T_f}{T_\infty}\right]^{0.17} \tag{3}$$

which is valid for Reynolds numbers Ud_w/ν_f up to about 45, where vortex shedding begins: for a 12.5 μm wire in air this corresponds to a speed of over 50 m s^{-1}, outside our range of interest.

The final differential equation that describes the temperature of the heated wire is

$$\frac{dT_w}{dt} = \frac{I^2 \chi_\infty}{A_w(\rho_w c_w A_w)} + \left\{ \frac{I^2 \chi_\infty \alpha_\infty}{A_w(\rho_w c_w A_w)} - \frac{\pi k_f Nu}{(\rho_w c_w A_w)} \right\} (T_w - T_\infty) \tag{4}$$

The wire time constant, M, can be written as

$$M = (\rho_w c_w A_w) \left\{ \pi k_f Nu - \frac{I^2 \chi_\infty \alpha_\infty}{A_w} \right\}^{-1} \tag{5}$$

The second term in Eq. (5) is very small compared with the first term and it can be neglected at very low overheat ratio or at high flow velocity. Therefore, the wire time constant, M, can be represented for these two parameters as

$$M = \frac{\rho_w c_w A_w}{\pi Nu k_f} \tag{6}$$

From Eq. (6), it follows that the wire time constant, M, decreases as Nusselt number, Nu, increases with flow speed.

After calculating the sending wire temperature as a function of time, the true time of flight was calculated by solving the time-dependent momentum, continuity and thermal energy equations for the flow over and behind a circular cylinder. The code, due to Perić (1988), handles variable fluid properties: details of the discretization procedure are given by Lange (1997).

Given the solution for the velocity and temperature on the wake center line at the position of the receiving wire, the variation of receiving wire temperature with time was calculated with the same code as the sending-wire response, but with the forcing in the heat-transfer term instead of the ohmic-heating term. The thermal energy balance for the receiving wire (Eq. (4)) can be written as

$$\frac{dT_w}{dt} = \frac{\pi Nu k_f}{(\rho_w c_w A_w)} (T_a - T_w) \tag{7}$$

where T_a is the ambient fluctuation temperature, which is detected in the heated wake by the receiving wire, and it has an approximately sinusoidal shape. The ambient temperature fluctuation, which is a function of the flow velocity, can be expressed as

$$T_a = T_m + \Delta T_a \cos(\omega t) \tag{8}$$

where T_m is the mean ambient temperature at the receiving wire; ΔT_a, the amplitude of the ambient temperature fluctuation; and ω, the angular velocity, which is equivalent to $2\pi f$, where f is the frequency of the ambient temperature fluctuation (and that of the sending-wire current) which is chosen as 30 Hz.

After substituting Eq. (8) in Eq. (7), a first-order ordinary differential equation is obtained, which can be integrated with respect to time to obtain the receiving wire temperature fluctuation in the following form:

$$T_w = T_m + \left(\frac{\Delta T_a}{1 + \omega^2 M^2}\right) [\cos(\omega t) + M\omega \sin(\omega t)] + C_1 e^{-t/M} \tag{9}$$

where C_1 is the integration constant which satisfies the initial condition.

Fig. 3 shows the relative importance of the three contributions to the time difference Δt at different speeds. The contributions of the sending and receiving wires are slightly different because of the different wire temperatures, and the corresponding differences of material properties of wire and fluid. The flattening of the time-of-flight curve at low speeds is due to longitudinal heat diffusion in the wire wake, and this sets the lower limit of usefulness of the present flowmeter at about 0.05 m s^{-1}.

The best separation distance, Δx, which gives the maximum velocity range was found to be 1.5 mm and therefore this value was chosen in the present sensor. The Peclet number (Pe) decreases as Δx between the wires reduces and therefore, the diffusion will have serious effects especially at low flow velocity. However, Δx cannot be chosen too large because the temperature signal in the fluid will be damped or vanish before it reaches the receiving wire, especially at high flow velocities.

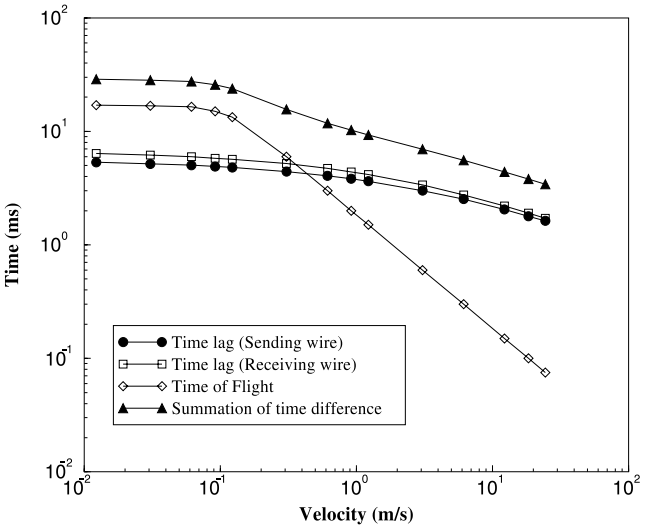

Fig. 3. The three components of the time difference and their summation versus the flow velocity (log scales).

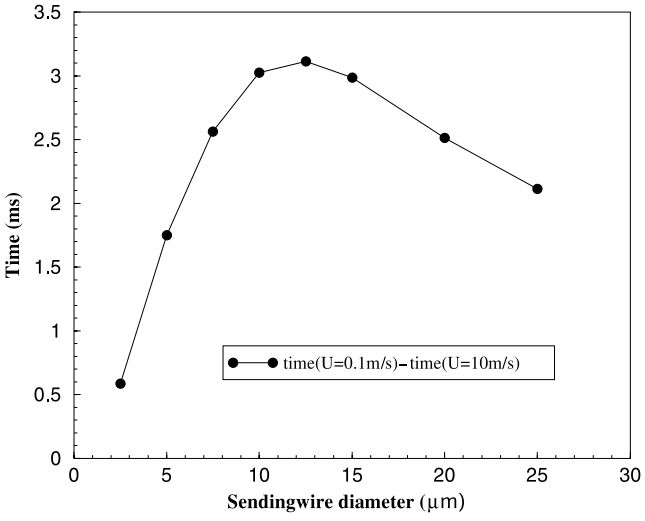

Fig. 4. The change in time difference over a given change of velocity ($0.1 \leqslant U_\infty \leqslant 10\ \mathrm{m\,s^{-1}}$) versus wire diameter for velocities of the order shown here.

Fig. 4 shows the change in time difference between $U = 0.1$ and $10\ \mathrm{m\,s^{-1}}$ (a representative value of the slope of the top curve in Fig. 3) over a range of wire diameters. This figure clearly shows that a wire diameter of about 12.5 μm is optimum for the kind of flow sensors described here.

It is preferable in practice to use platinum wires, which can be operated at higher temperature than, say, tungsten without oxidizing. Platinum is not as strong as tungsten, so the latter is preferred for conventional hot-wire anemometry with wires of 5 μm diameter or less; with our larger wire diameters, strength is not so important. Also, it is easy to handle and is available in a wide range of diameters at an affordable price.

3.3. The driving current frequency

The maximum permissible frequency, f, of the driving current must be an order of magnitude lower than the reciprocal of the sending wire time constant (M), to avoid severe attenuation of the temperature variation in the sending wire. Therefore, the maximum current frequency can be expected to be of the order of 100 Hz or less for the given parameters.

The strong dependence of amplitude of the sending wire output temperature signal on the driving current frequency at a given velocity is shown in Fig. 5. The magnitude of the temperature fluctuation of the wire is less than the magnitude of the forcing input signal by the factor $1/(1 + M^2\omega^2)^{1/2}$. In addition, the temperature response of the sending or receiving wire is shifted in phase with respect to the forcing function by an amount depending upon the time constant and the frequency as shown in Eq. (10):

$$\Delta\phi_{\mathrm{shift}} = \omega\Delta t_{\mathrm{shift}} = \arctan(M\omega) \tag{10}$$

The maximum time difference in each wire will be limited by the above equation to one quarter of the reciprocal frequency, $1/(4f)$, i.e. a phase shift of 90°. If $\omega = 1/M$: then the magnitude of the temperature fluctuations is smaller than that of the forcing function by $1/\sqrt{2}$, and the phase shift is 45°.

It is recommended that one should obtain an output temperature signal with large amplitude to extend the dynamic range of the sensor. Therefore, it is essential that the current frequency of the sending wire be as small as possible. Also, it is noted that the sending-wire phase shift does not matter (much), so all that is needed is for $1/(1 + \omega^2M^2)^{1/2}$ to be not too small compared with unity; 0.7 would be acceptable and one can obtain that with $\omega M = 1$, a frequency of 30 Hz which is suitable for the application of the present sensor to tasks such as the measurement of breathing of animals.

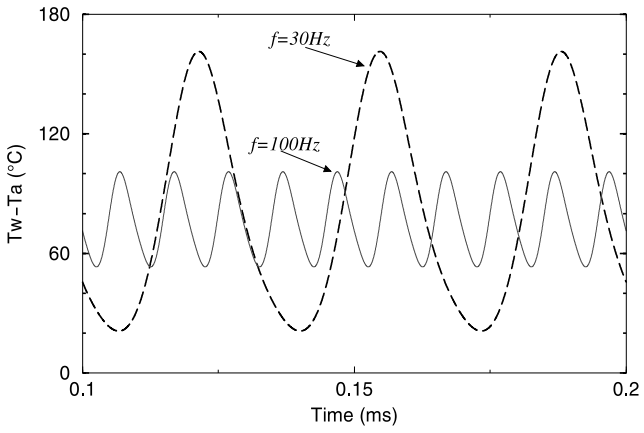

Fig. 5. The response of the sending wire to varying frequencies of a supply current is plotted as ΔT (°C) versus time (ms).

4. Experimental data

This section describes in detail the test probes and electronics that were built according to the theoretical results of Section 3. It also provides a short description of the measurement setup for the characterization and calibration of the thermal flow sensor and summarizes the experimental results obtained for different cases.

4.1. Realization of sensor

The thermal flow sensor was designed and built to measure the flow velocity and the volume flow rate of different gases in pipe flow under a wide variety of conditions. This design is shown in Fig. 6a, in which two parallel wires are placed in the probe throat area. The selected wire diameter should be large enough to obtain a robust wire since the wires are prone to breakage. For most applications, a comparatively robust sensor is preferable. This is important in terms of lifetime, long-term stability of the calibration and the effect of contamination. The first wire is the sending wire which is heated by an oscillating current at 30 Hz frequency. The selected length of this heated wire is 5 mm, which is three times greater than the separation distance between the two wires, and its optimization diameter is 12.5 μm as shown in Fig. 4.

Regarding the receiving wire, which detects the temperature variation in the wake of the first heated wire, it is located at a distinct distance equal to 1.5 mm and its diameter and its length are similar to those of the sending wire. It would appear that there is a strong motive to reduce the spacing between the wires as much as possible, and this would also be helpful in reducing the size of the probe. However, the diffusion effect sets a broad limit on the permissible reduction of this spacing. It does not seem advisable to reduce the Peclet number by reducing spacing between the wires since the minimum measurable velocity is set by thermal diffusion effects.

Both the sending and receiving wires of the thermal flow sensor were manufactured from platinum, which is a suitable material especially for the sending wire because it is capable of operating at high temperature without oxidizing. Obviously, platinum loses strength when it becomes really hot, but a large diameter was just a satisfactory result of the optimization process, giving increased strength at any temperature.

The probe body, which contains the sending wire and the receiving wire, is shown in Fig. 6b. The probe was designed in such a way as to ensure that the incoming velocity profile is uniform over the whole cross-section of area at which the sending and receiving wires are located. Thus the average velocity of the incoming flow, and consequently the volume flow rate, could be measured. Therefore, a nozzle shape is selected to achieve a uniform velocity distribution with low turbulence at the throat area where the two wires are fixed.

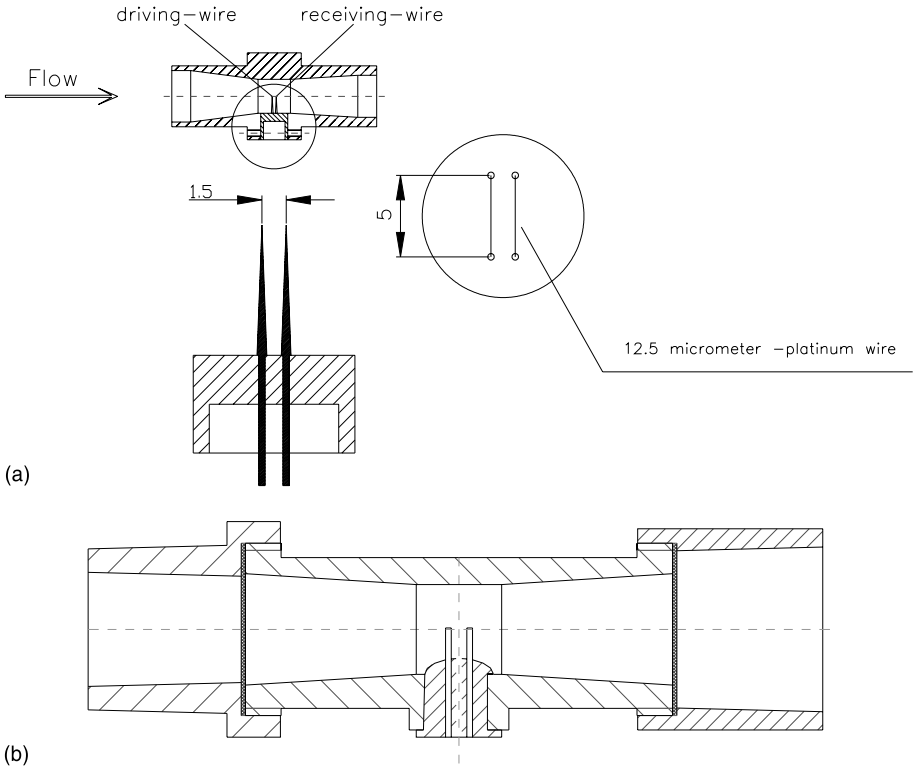

Fig. 6. (a) The probe design of the two-wire thermal flow sensor. (b) Schematic of the probe casing.

Accordingly, the test probe, which is shown in Fig. 6b, consisted of a nozzle and a diffuser in one unit and has a diameter of 12.5 mm at the throat area. It was made of Plexiglas, and at the place where the nozzle outlet and the diffuser inlet meet, the two wires, which were soldered on the prongs, are installed. Fig. 6a and b show the final design of the test probe sensor used in the present investigation.

The ends of both wires were soldered on the tips of the holding prong precisely and accurately. The amount of tin for soldering the hot wire to the holding prongs is also very important, not only due to heat transfer phenomena but also so as not to disturb the incoming flow.

4.2. Electronic circuit

A block diagram of the circuit for the two-wire probe is shown in Fig. 7 (copies of the detailed circuit diagram may be obtained from the senior author). Essentially this is a phase-locked-loop circuit which detects zero crossings in the ac part of the "receiving" wire voltage.

Blocks (1)–(4), at the top of Fig. 7, provide the ac part of the sending wire voltage, the usual frequency being 30 Hz, and also send a 30 Hz square-wave train to the phase shifter (5), whose only purpose is to compensate for the inevitable phase shift in the filter (4). The filter is a switched-capacitor type, driven by a clock pulse at a frequency which is an exact multiple of the main (30 Hz) square-wave input: this type of filter can convert square waves into sine waves with very small harmonic distortion, at the cost of attenuation of the signal.

Block (7) provides the dc part of the sending wire voltage. Because the power dissipation depends on the square of the voltage, a voltage which had a positive mean but some negative intervals would introduce harmonics of the basic frequency. The optimum, producing the least mean power input, is a voltage which just stays positive, and the adjustment is made in block (7), the ac and dc voltages being summed in block (6). The operational amplifier (8) provides a current source for the sending wire (9), typically up to 100 mA, and it is also used to amplify the voltage from the filter: the more accurate the filter the more it attenuates the signal.

Blocks (10)–(12) need little explanation. The receiving wire current is typically set at 3–7 mA. The amplifier gain is set to give adequately large voltage inputs to the phase-locked loops (13) and (14). The actual voltage is almost immaterial, because the phase-locked loops detect zero crossings of the AC part of the periodic input voltage PLL1 with a very small threshold. The first phase-locked loop, (13), converts the receiving wire output signal, which is not quite sinusoidal and is inevitably noisy, into a square wave whose successive

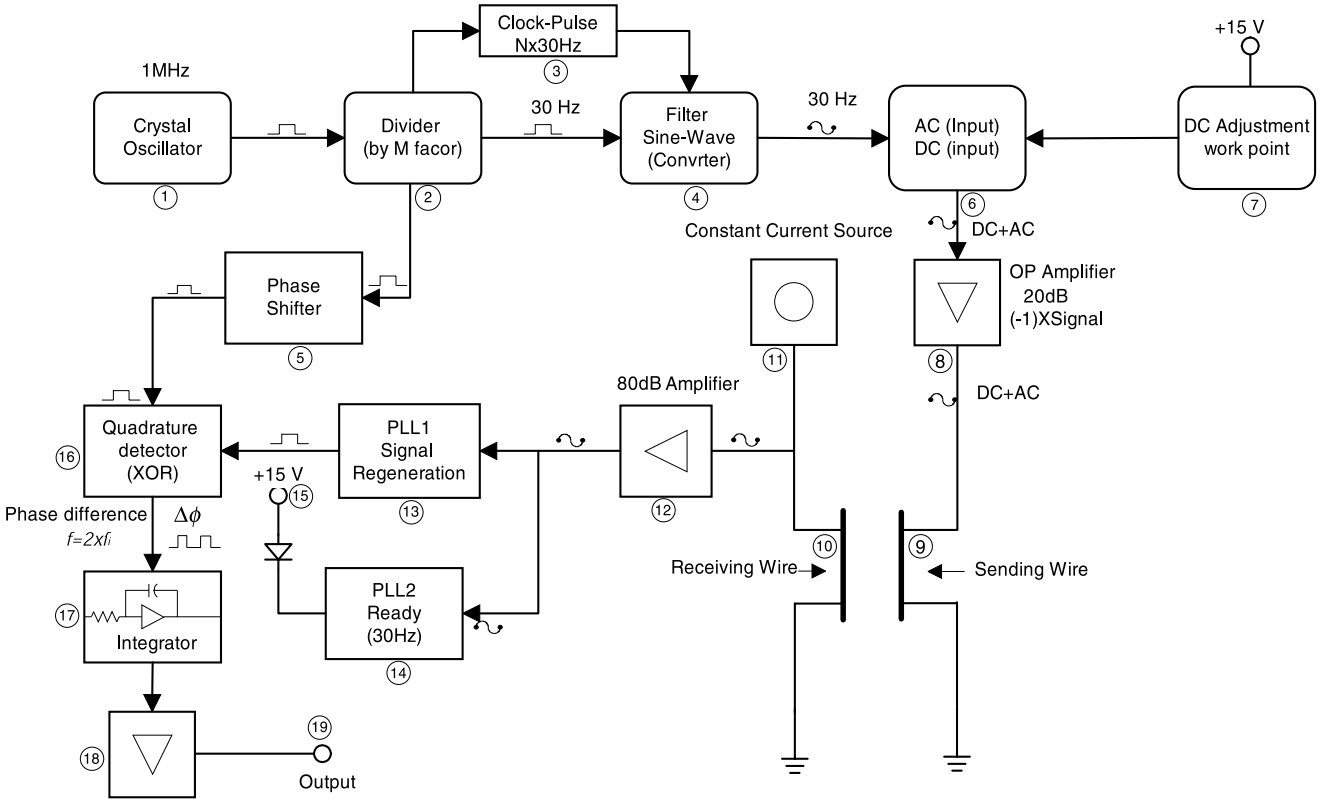

Fig. 7. The block diagram for the electronic circuit.

leading edges are at exactly 30 Hz. Variations in the time between zero crossings appear as phase shifts rather than changes in frequency. This is much less critical than the corresponding process in pulsed-wire anemometry. There, the apparent time of flight depends strongly on the threshold set to detect departure of the receiving wire voltage from its value at ambient temperature. The reason is that the departure is initially quadratic: in our case the voltage varies linearly near the detection point (zero crossing). The second phase-locked loop, (14), repeats the operation of the first and then checks to see if the output square wave is acceptable: if so, the green light-emitting diode (15) is illuminated.

The "quadrature detector" (15) simply produces the exclusive OR (XOR) of the square-wave output of PLL1 and the square-wave output of the phase shifter (5). Note that these are effectively on–off logic signals as well as analog waveforms. The phase difference between the two waveforms is the phase difference between the sending wire input and the receiving wire output and is therefore proportional to the total "time of flight". The larger the phase difference (always $<90°$) the longer the intervals in which the XOR logic signal is true: it is obviously never true if the two square waves have zero phase difference. This logic signal, now regarded as an analog wave form, is fed into the integrator (17). After a given integration time large compared to 1/30 s (say 2 s), the integrator output is the phase shift averaged over that time. The flowmeter is calibrated to relate the integrator output to the flow speed or flow rate.

After the measurements reported here were completed, an improved method of integration was developed. The modified circuit is shown in Fig. 8. The quadrature-detector logic output is sampled at 250 kHz by a digital-to-analog converter synchronized to the XOR cycle, and the analog voltage is integrated, one cycle at a time. The advantage is that a velocity reading is obtained every cycle, that is, at a rate of 30 Hz. Because the DAC sampling rate is finite, so is the *minimum* phase shift (*maximum* flow speed) that can be measured to given accuracy. The 250 kHz rate is, however, adequately high for our purposes. If we require 100 DAC samples during the shortest XOR "true" output pulse for our probe with a wire spacing $\Delta x = 1.5$ mm (1% nominal accuracy) and recall that the apparent time of flight is roughly $3\,\Delta x/U$, we find that a DAC sampling rate of 250 kHz allows phase-shift measurement to 1% accuracy for $U_\infty < 30\ \mathrm{m\,s^{-1}}$.

Integration of a pseudo-analog XOR output is a convenient form of signal analysis, but there are several

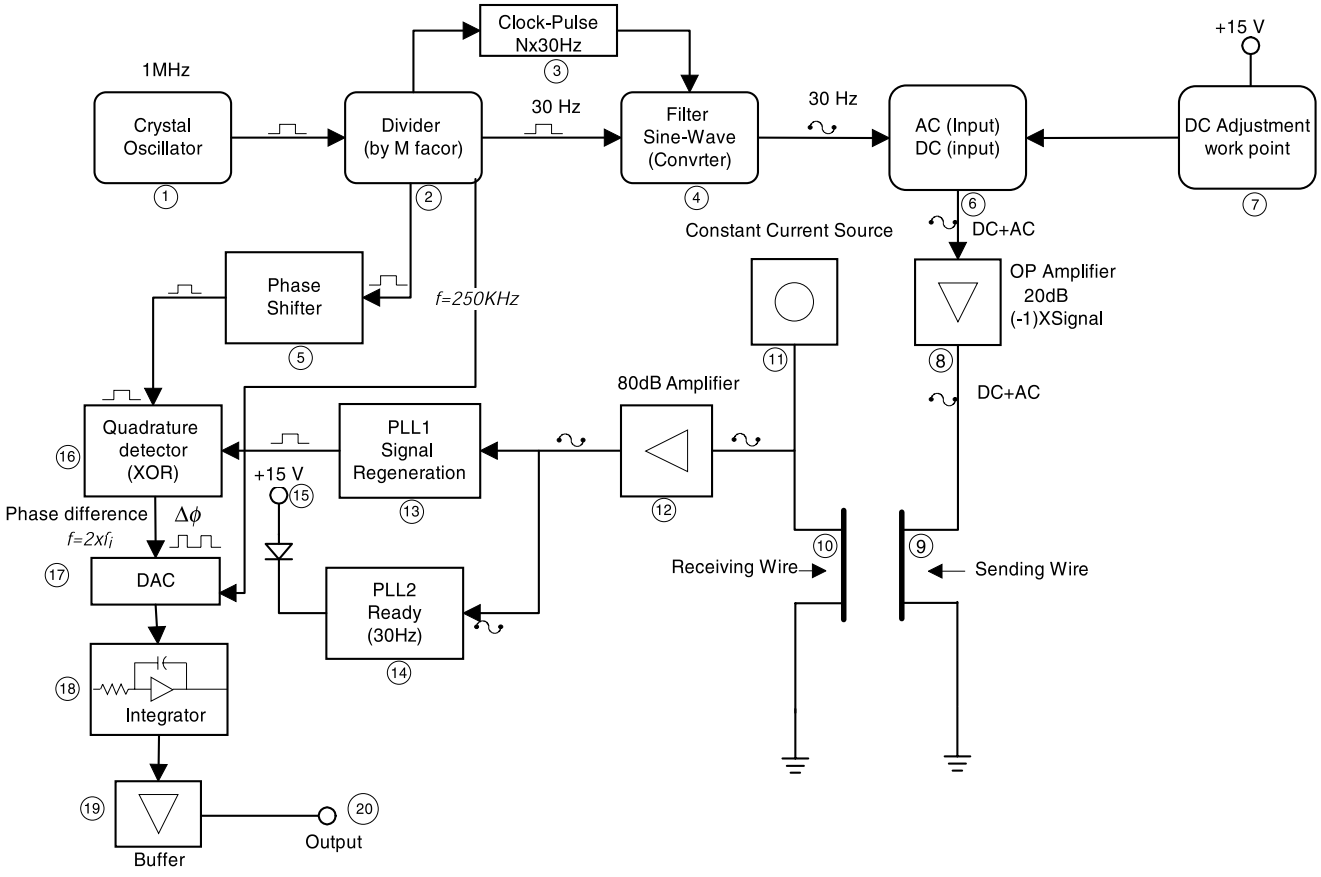

Fig. 8. The block diagram for the electronic circuit in which an improved method of integration was developed.

related analog or digital methods of measuring the phase (time) difference between the leading edges of the two signals at each cycle.

4.3. Calibration facilities and measuring equipment

4.3.1. Wind tunnel and LDA system

To calibrate the thermal sensor described in Section 4.1, some measurements were performed in a small wind tunnel with a laser Doppler anemometer as velocity reference, the accuracy of which is estimated to be less than $\pm 0.1\%$ of the reading.

The wind tunnel was arranged and optimized to yield a constant blowing rate through the fan and a velocity range between 0.1 and 30 $\mathrm{m\,s^{-1}}$ can be realized with a background turbulence of $<1.0\%$. The air from the fan passed through a diffuser, followed by two sets of 90° corner guide plates, prior to passing the heat exchanger and then to the settling chamber of the wind tunnel. An air–liquid heat exchanger was installed in front of the settling chamber and before the test section in order to heat or cool the air, which is in circuit, between −4 and +60 °C. Also, the heat exchanger can keep the temperature of the air flow inside the wind tunnel at a certain value during the experiment irrespective to the variation of the ambient temperature. After the air flow has passed through the heat exchanger, it passes through a settling chamber to stabilize and stream it and then through an optimized contraction nozzle to achieve a uniform and high velocity in the working test section. From there the flow enters the wind tunnel test section with its major dimensions being $\mathrm{W} \times \mathrm{H} \times \mathrm{L} = 200 \times 200 \times 300$ $\mathrm{mm^3}$. To provide optical access for the employed laser Doppler system, all sides of the wind tunnel test section are made of Plexiglas. This permitted the laser beams to pass and intersect on the desired point of measurement where the probe is located without disturbing the flow.

The laser Doppler optical system employed was operated in the dual-beam forward-scattering mode. The LDA system used was a one-component system consisted of a laser beam with an 18 mW He–Ne laser (wavelength = 0.6328 μm). The prism causes laser beam to split into two equal-intensity, parallel beams and the distance between these two beams is $d = 60$ mm. Then the two beams are well focused inside the measuring volume through a focusing lens of the transmission optics with a focal length of $f = 310$ mm. The optical arrangement was laid out to yield a measuring control volume, based on the e^{-2} Gaussian light intensity cut-off point, of 380 μm in diameter and 3.9 mm in length. The light scattered in the forward direction by small liquid particles moving through the measuring volume in the air stream was collected by the receiving optics and focused on to an appropriately sized pinhole of 100 μm diameter located at the front of an avalanche photodiode. The particles were very tiny liquid droplets and they consisted of alcohol and water, with diameters of 0.5–2 μm and mean diameter $d = 1.068$ μm. The wind tunnel was filled with fog fluid and approximately 1 min after the end of fog generation the measurements were started.

4.3.2. Calibration facility for a very low-velocity air flow

For calibration at low velocity, a laboratory-made calibration facility made at LSTM—Erlangen was used. The flow rate is measured by a special LDA or by periodically recording the weight of water in a small container. Fig. 9 shows a schematic diagram of the water container that used for low flow rates, say <3.0 l/min (the flow velocity is <0.5 $\mathrm{m\,s^{-1}}$). In this technique, the water is allowed to flow from the bottom of a large enclosed tank with a probe inserted in an opening at the top through which air enters as shown in Fig. 9. The thermal flow sensor is placed at the air inlet on the top channel and it is connected with a long, straight pipe containing a screen with very small mesh sizes to attenuate the fluctuations and to take the measurements with a uniform, fully developed incoming flow without any disturbances.

The inlet to the sensor test section has a smooth nozzle shape in order to obtain a uniform velocity distribution at the wire position. The channel at the bottom is opened and a quantity of water will flow through the channel and will be collected and weighed by using an electrical digital balance during a certain time. The volume of water is equal to the volume of air which replaces it in the tank. The estimated uncertainty in the air flow velocity from the water vessel was calculated and found to be about 1% from the measured value. An advantage of this method is that a very low air flow velocity can be measured and dry air passes over the probe.

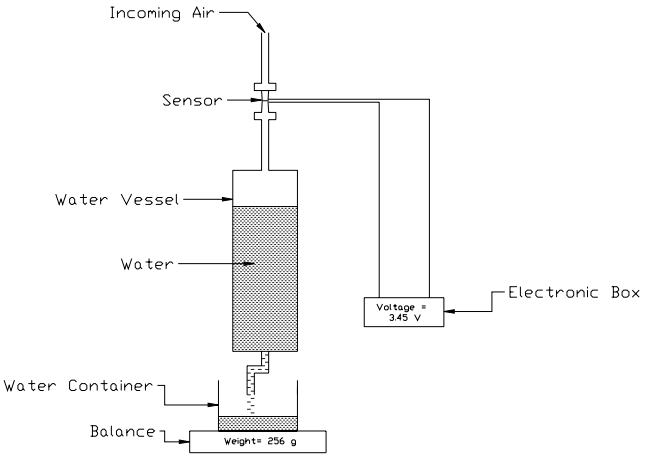

Fig. 9. Schematic diagram of the water tank used for low-velocity calibration.

4.4. Experimental results and comparisons

4.4.1. Sensor calibration

Owing to the non-linear behavior of the thermal flow sensor, calibration over the whole speed range is necessary. Although in principle this is a disadvantage, it is at the same time an advantage to have a non-linear transfer function giving high accuracy at the lower end of the range.

A large number of measurements were made to test the feasibility of the operating technique. The measurements were carried out with probes similar to that shown in Fig. 6a. The procedure that was followed here for representing our experimental data is based on measuring the voltage which results from the integration of the phase shift between the sending and receiving signals. The mean-flow calibration obtained from the position of the wire intercepts of the thermal sensor ($\Delta x = 1.5$ mm) is shown in Fig. 10. The first experimental results, presented here, are considered to be satisfactory since they represent a behavior confirming the theoretical analysis in Section 3 (Fig. 3). The calibration was carried out over the range from very low velocities (down to 0.05 $\mathrm{m\,s^{-1}}$) to moderate velocities (up to 25 $\mathrm{m\,s^{-1}}$). The results show that the present sensor can cover the whole dynamic range of 500:1 with high accuracy and sensitivity (inaccuracy <3%).

It should be noted that the results obtained in this section are taken from a more general investigation of the relation between the flow velocity of the working fluid and the response of the thermal flow sensor. However, only those results which contribute to the present discussion about the calibration results for the thermal flow sensors have been included. Many measurements for various combinations of wire diameters, different separation distances between the sending and the detecting wires and different operating conditions have been conducted to obtain the final optimized design for the present sensor.

Measurements for various combinations of flow conditions such as various ambient temperatures, different air humidities and dissimilar gas components have been made and the results are summarized in the following subsections. Verification of the experimental data with the computed results will be demonstrated at the end of this section. First, measurements of long-term stability (repeatability) which check the reliability of the present sensor will be presented.

4.4.2. Repeatability

Repeatability represents the capacity of the flow-rate meter to reproduce the same readings which are very similar to each other for the same flow rate value, under the same operating condition. Of course, good reliability does not imply the goodness of the instrument readings.

One of the major problems with hot-wire anemometers is long-term stability. This is especially the case when the sensing element is made very small to give a fast time response. Short-term drift in the hot wire occurs as a result of air temperature changes and dirt accumulation and long-term drift results from metallurgical changes to the wire. It is well known from hot-wire anemometry that calibration of the wire is necessary at relatively short time intervals, perhaps several times a day. The reason for this is the relatively large change in heat exchange from the wire to the surroundings, when the ambient temperature drifts slightly or when the wire is contaminated. Even in environments with relatively clean gas, contamination can occur.

The sensor described here does not suffer from this problem, because its operation depends on the phase shift between the sending and receiving signals and it is nearly independent of the outside conditions such as the ambient temperature. To verify this statement, a number of tests were carried out. The same calibration results were maintained after several days of operation with an error of <3%. Fig. 11 demonstrates the independence of the calibration curve for the present sensor of the out-

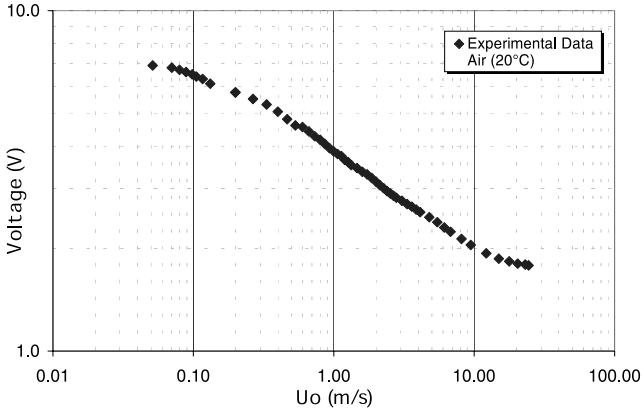

Fig. 10. Calibration curve for determining the velocity as a function of the output voltage.

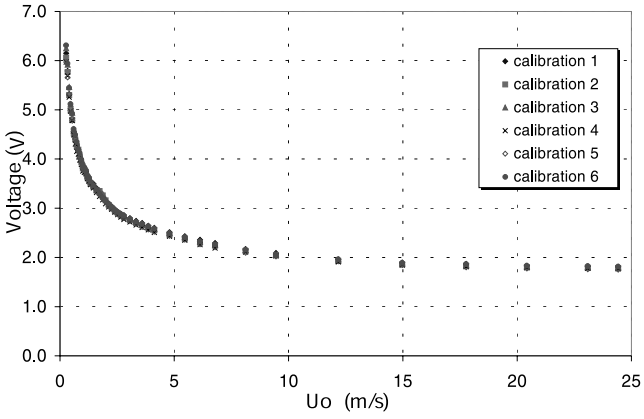

Fig. 11. The long-term stability of the thermal flow sensor.

side conditions and its repeatability. Also, one can conclude from Fig. 11 that the repeatability of this sensor is very high and therefore this device is sufficient for many applications.

The sensitivity and accuracy of the present sensor are very high at low flow velocities because of the non-linear transfer function of the thermal flow sensor as shown in Figs. 10 and 11. The sensitivity of the measured velocity is approximately 0.3% at low flow velocities and it increases with velocity to reach 3% at high velocities.

4.4.3. Influence of the ambient temperature

The aim of this section is to investigate the influence of ambient temperature on the time difference between the sending and receiving signals from the wires and particularly on the calibration curve of the thermal sensor. A special experimental setup which permitted closely controlled variation of the flow air temperature was used. The output results were compared with the reference calibration curve at normal ambient conditions ($T_a = 20$ °C). The results in Fig. 12 show that there are small differences between the typical calibration curve and the measurement results at different ambient temperatures. The observed difference is very small and to understand this deviation it is necessary to know how the fluid properties (density, viscosity, thermal conductivity, specific heat, etc.) depend on temperature. The time constant of both wires and therefore the output voltage of the thermal sensor were found to decrease slowly with increasing ambient temperature, as one can see from Fig. 12. Our previous analysis showed that the time difference between the two signals, and thus the output voltage from the thermal sensor, are directly proportional to the density and the specific heat of the flow and inversely proportional to the Nusselt number of the wires and the thermal conductivity of the fluid at a constant wire diameter (see Eq. (6)).

According to the data correlation of Collis and Williams (1959), the Nusselt number varies linearly with (Reynolds number)$^{0.45}$. The Reynolds number decreases with increasing flow temperature at a certain velocity because of the increase in the fluid viscosity. The wire time constant varies as $1/Nu$ and the Nusselt number decreases with increasing temperature. On the other hand, the temperature correction factor for the Nusselt number increases with increasing ambient temperature. However, the thermal conductivity of the fluid, which, together with the Nusselt number, is in the denominator of the time constant relation, is related to the absolute temperature approximately as $k_f \propto (T_{abs})^{0.75}$, and therefore it will cause the time constant to decrease. However, the density of the fluid is inversely proportional to the ambient temperature and therefore it will contribute to reducing the time constant of both wires with temperature. The specific heat of the sensor wires is very weakly dependent on the ambient temperature. The time-of-flight component can be accurately found to be independent of the ambient temperature over a wide velocity range except at very low flow velocities where the diffusion effect plays a major role. The diffusion time is inversely proportional to the thermal diffusivity, which increases with increase in temperature. Thus, the final time difference between the two signals and/or the final output voltage (integration of the phase shift) vary very slowly with the ambient temperature and they are only very weakly dependent on the temperature, as shown in Fig. 12, which covers a wide range of investigated ambient temperature between 0 and 60 °C.

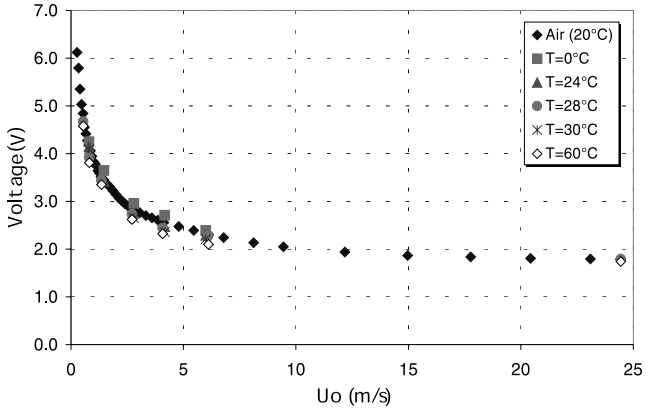

Fig. 12. The calibration curve of the flow thermal sensor in the temperature range 0–60 °C.

The time shift or the integrated output voltage decreases linearly with increasing ambient temperature. Therefore, the calibration results for air at low ambient temperature ($T_a = 0$ °C) are located above the typical calibration curve for air ($T_a = 20$ °C), whereas the calibration results for air at high ambient temperature ($T_a = 60$ °C) are located below the typical curve as shown in Fig. 12. The small deviation provides strong evidence that the accuracy of the thermal flow sensor is very high under a variety of ambient conditions. The maximum error in the velocity due to the variations of the ambient temperature will be <0.75% per degree if the flow velocity is larger than 4.0 m s^{-1}. However, this error is directly proportional to the flow velocity and reaches less than 0.2% at a flow velocity of 0.5 m s^{-1}.

4.4.4. Influence of gas composition

Since the response of the thermal flow sensor is only very weakly dependent on fluid density, the thermal flow sensor can be effectively used in flows of gas mixtures. A good example is given in Fig. 13, which shows the calibration for air and other gas compositions. Many different cases were surveyed in which the flow gas was different to the ambient gas such as: (i) pure nitrogen (N_2); (ii) pure oxygen (O_2); (iii) nitrogen and nitrogen monoxide (97% N_2 + 3% NO); and (iv) nitrogen and oxygen (92% N_2 + 8% O_2).

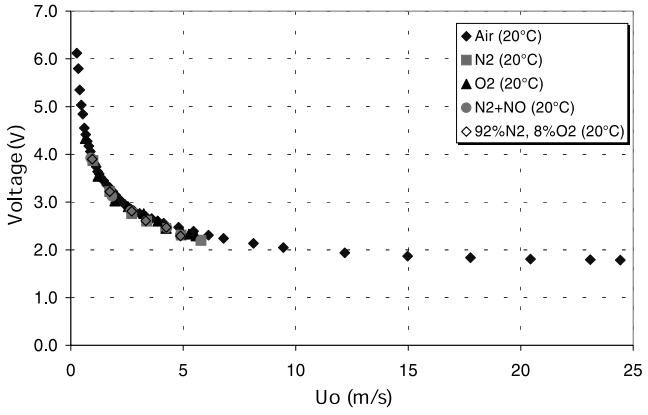

Fig. 13. The calibration curve of the flow thermal sensor for different gas components.

4.4.5. Influence of the air humidity

To investigate the influence of humidity on the time difference between the sending and receiving signals, a special experimental setup which allowed control of the gas temperature and humidity was constructed at the LSTM—Erlangen laboratory. The measurements were carried out for a wide range of different fluid velocities. The relative humidity was changed from 5% to 70% and back to 5% or 10%. Each measurement cycle was performed at constant temperature and humidity, while the velocity was changed from low to high and back to low.

Fig. 14 shows the influence of air humidity on a typical calibration curve of the thermal flow sensor. There is a small deviation between the measurement results at different relative humidity and also a small deviation from the typical calibration curve can be observed. This deviation is $<0.15\%$ per 1% humidity change at high velocity and this error decreases as the flow velocity decreases. The output voltage and therefore the measured velocity decrease slightly as the relative humidity increases.

The heat transfer from the heated wire to the fluid increases with increasing humidity. Still et al. (1998) found experimentally that the ratio of the heat transfer rates in humid air and dry air is a unique function of the molar fraction of water vapor, and it is independent of the air temperature and flow velocity. Therefore, the output voltage of the thermal flow sensor decreases linearly with increasing relative humidity, i.e. the time shift between the sending and receiving signals decreases as the humidity increases. However, as we can see from Fig. 14, the influence of air humidity on the typical calibration curve is very small and can be neglected.

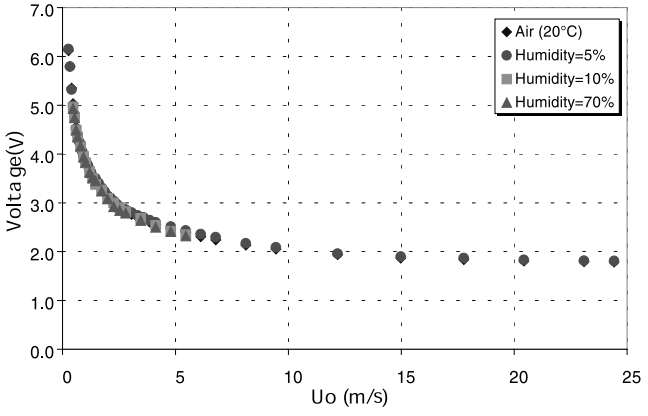

Fig. 14. The calibration curve of the flow thermal sensor in the relative humidity range 5–70%.

4.4.6. Comparison of experimental and theoretical results

Our measurements confirm the calculations to within the expected accuracy. We emphasize that individual calibration of probes is necessary for the highest accuracy: wire diameters in the micron range cannot be precisely controlled, nor can wire spacing. However our best estimates of the likely error (97% certainty) due to variations in wire diameter and spacing are only 3%, which may be adequate for many purposes.

The experimental data were compared with the theoretical results derived in Section 3. The comparison shown in Fig. 15 indicates excellent agreement between the theoretical and experimental results. This agreement is very good not only at high but also at low velocity. The velocity attainable range is 0.05–25 $\mathrm{m\,s^{-1}}$ and the error between the measurements and the computations is $<3\%$. Also, several series of measurements have shown very good reliability (of the order of 3%). At the highest velocity ($U_\infty \geqslant 0.7\ \mathrm{m\,s^{-1}}$ and $Pe \geqslant 50$), the agreement between the numerical and experimental results was very good, and the results were typical of those in which the effects of thermal diffusion are small. However, the results showed that the time difference between the sending and receiving signals increases gradually at low velocities ($U_\infty \leqslant 0.1\ \mathrm{m\,s^{-1}}$). This behavior verifies the leading role of diffusion in the case of low flow velocity.

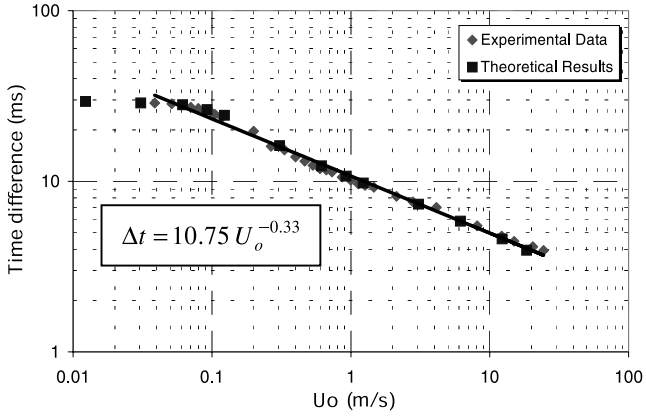

Fig. 15. Comparison between experimental and computed results for the thermal flow sensor in different gaseous flows drawn on log scales. (It can be seen from this figure that the experimental results correlate very well with the theoretical predictions.)

The dominance of diffusion over transport became more important as the velocity became lower. On the other hand, the numerical calculations at lower velocities show that thermal diffusion effects are very large and have a strong influence on the apparent time of flight. The minimum measured velocity was 0.05 m s^{-1}. It will be very difficult to measure a flow velocity which is less than this value, since the time difference between the sending and receiving signals will be nearly constant and the thermal diffusion time will be dominant.

Fig. 15 shows that the time shift between the sending and receiving signals at $U_\infty > 0.1$ m s^{-1} is approximately inversely proportional to the one-third power of the flow velocity ($\Delta t \propto U_\infty^{-0.33}$, we do not suggest that the power is exactly 1/3), whereas the time-of-flight component is inversely proportional to the flow velocity ($\Delta t_f \propto U_\infty^{-1}$). Therefore, the dynamic range of the measured velocity with the present sensor is high and it is larger than that of the pulsed-wire anemometer, which measures only the time of flight to determine the flow velocity.

5. Conclusions

We have developed a two-wire sinusoidally excited "time-of-flight" flowmeter whose speed range is increased by deliberately using large-diameter sending and receiving wires, whose thermal lag adds to the time lag due to the true aerodynamic time of flight. Our present device, using 12.5 μm platinum wires, has a usable range from 0.05 to 25 m s^{-1}. With 30 Hz excitation, the frequency response is nominally 15 Hz.

The main advantage of the two-wire thermal flow sensor over the hot-wire anemometry is its low sensitivity to variations in temperature and also to the composition of the flowing gas. Also, calibrations for use in flows of variable density are unnecessary, so velocity measurements in gas mixtures are relatively straightforward.

As well as exploring a range of sensor parameters, we have calculated the effect of changes in atmospheric temperature, humidity and gas composition on the flowmeter response. As expected, these effects are small within the (arbitrarily chosen) ranges explored. The calculations could be used to adjust calibrations obtained in room-temperature air for, say, use in warm exhaled breath containing carbon dioxide and water vapour.

A sample calibration of Δt against U_∞ is compared with the corresponding prediction in Fig. 15. So far from being proportional to $1/U_\infty$, Δt is seen to be proportional to $U_\infty^{-0.33}$ approximately. The decreased gradient of Δt against U_∞ at the lowest speeds may be blamed on longitudinal diffusion, with some suspicion falling on buoyancy.

Acknowledgements

Without Herr Horst Weber's knowledge of practical electronics and his skill in circuit design, this project would never have come to completion. A. Al-Salaymeh was financially supported by the German Exchange Service (DAAD) when carrying out this research.

References

Al-Salaymeh, A., 2001. Flow velocity and volume flow rate sensors with a wide band width. Ph.D. Dissertation, Technischen Fakultät der Universität Erlangen-Nürnberg.

Collis, D.C., Williams, M.J., 1959. Two-dimensional convection from heated wires at low Reynolds number. J. Fluid Mech. 6, 357–384.

Durst, F., Al-Salaymeh, A., Jovanovi, J., 2001. Theoretical and experimental investigations of a wide range thermal velocity sensor. Meas. Sci. Technol. 12, 223–237.

Handford, P.M., Bradshaw, P., 1989. The pulsed-wire anemometer. Expt. Fluids 7, 125–132.

Kovasznay, L.S.G., 1949. Hot-wire investigation of the wake behind cylinders at low Reynolds numbers. Proc. Roy. Soc. London A 198, 174–190.

Lange, C.F., 1997. Numerical predictions of heat and momentum transfer from a cylinder in crossflow with implications to hot-wire anemometry. Ph.D. Dissertation, Technische Fakultät der Universität Erlangen-Nürnberg.

Perić, M., 1988. Comparison of finite-volume numerical methods with staggered and colocated grids. Comput. Fluids 16, 389–403.

Still, M., Venzke, H., Durst, F., Melling, A., 1998. Influence of humidity on the convective heat transfer from small cylinders. Expt. Fluids 24, 141–150.